**SUPPLEMENTARY INFORMATION**

# Ceramide targets autophagosomes to mitochondria and induces lethal mitophagy

R. David Sentelle[1,2,#], Can E. Senkal[1,2,#], Wenhui Jiang[1,2], Suriyan Ponnusamy[1,2], Salih Gencer[1,2], Shanmugam Panneer Selvam[1,2], Venkat K. Ramshesh[2,3], Yuri K. Peterson[2,3], John J. Lemasters[2,3], Zdzislaw M. Szulc[1,2], Jacek Bielawski[1,2] & Besim Ogretmen[1,2,*]

[1]Departments of Biochemistry and Molecular Biology, and [3]Pharmaceutical Sciences, and [2]Hollings Cancer Center, Medical University of South Carolina, 86 Jonathan Lucas Street, Charleston, SC, 29425, USA

[*]To whom correspondence should be addressed: E-mail: ogretmen@musc.edu; Fax: 843-792-2556.

[#]These authors contributed equally to this project

## SUPPLEMENTARY RESULTS

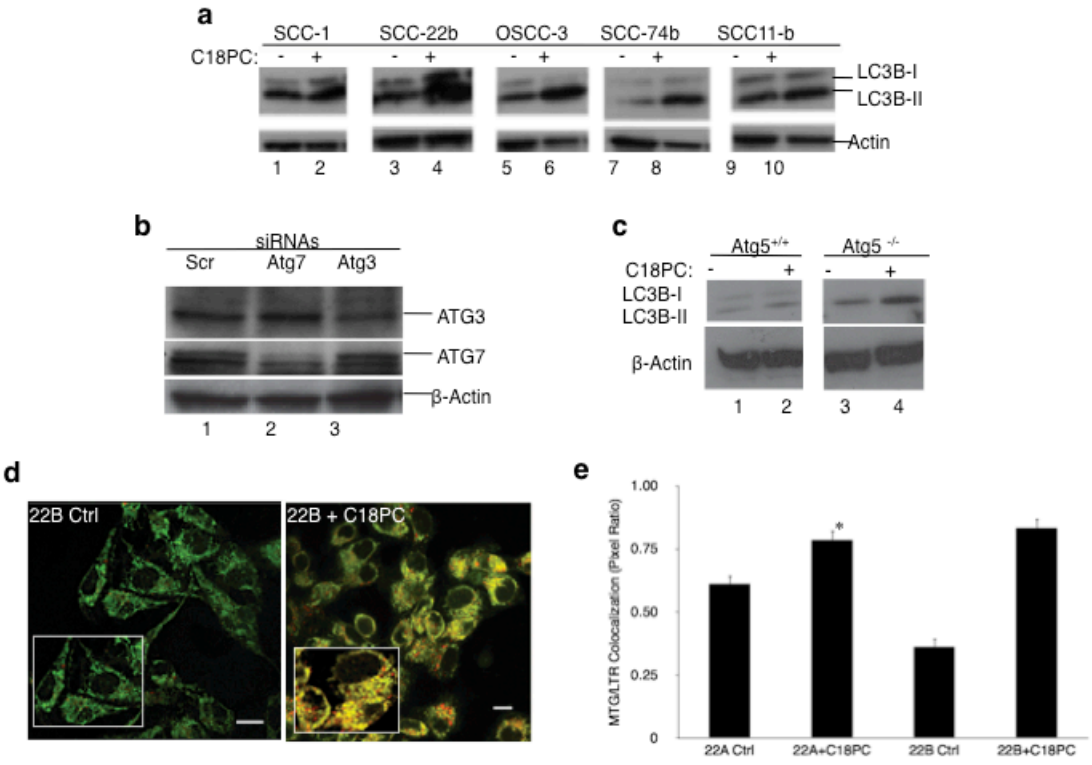


**Supplementary Figure 1.** $C_{18}$-Pyr-Cer induces LC3B-lipidation in multiple HNSCC cell lines, and wt MEFs but not in ATG5-/- k/o MEFs. **(a)** Lipidation of LC3B in response to $C_{18}$-Pyr-Cer was detected in SCC-1, SCC2b, OSCC-3, SCC24b, and SCC11-b cells by Western blotting, compared to vehicle-treated cells (lanes 2-1, 4-3, 6-5, 8-7, and 10-9, respectively). Beta-actin was used as a loading control. **(b)** Selective knock-down of Atg7, and Atg3 using siRNAs were confirmed by Western blotting (lanes 2-3 and 1, respectively). Beta-actin was used as a loading control. **(c)** Effects of $C_{18}$-Pyr-Cer on LC3B-II formation were examined in wt and ATG5-/- MEFs by Western blotting, compared to controls (lanes 2-1 and 4-3, respectively). **(d-e)** Targeting of autophagolysosomes to mitochondria in the absence/presence of $C_{18}$-Pyr-Cer at 2 h in UM-SCC22B cells was examined by visualizing the co-localization of MTG and LTR using live cell imaging and confocal microscopy (d). Scale bars represent 10 microns (d). Correlation R values for MTG and LTR co-localization IN UM-SCC-22A and UM-SCC-22B cells were obtained using Olympus software (e). Data shown are an average of at least two independent experiments performed in duplicates ± s.d. (*$P$ <0.05).

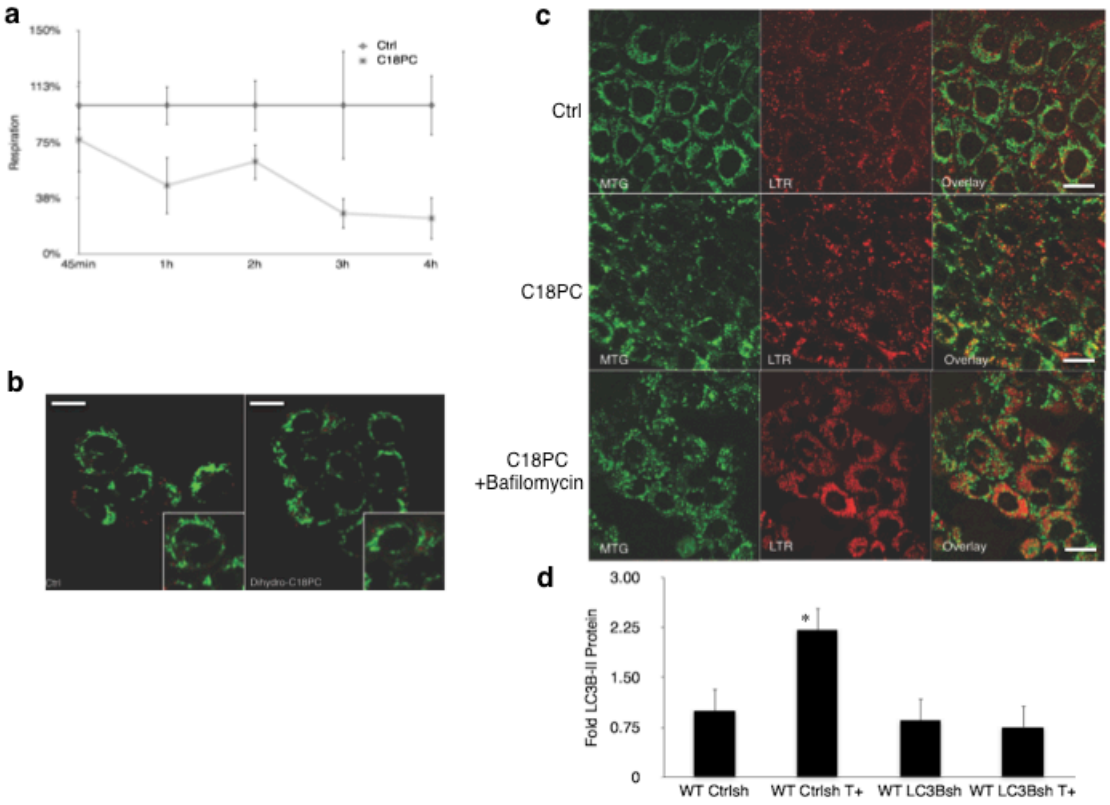


**Supplementary Figure 2.** $C_{18}$-Pyr-Cer or CerS1/$C_{18}$-ceramide, but not dihydro-ceramide analogue, decreases OCR and increases LC3B lipidation without affecting lysosomal flux in UM-SCC-22A cells. **(a)** Inhibition of OCR by $C_{18}$-Pyr-Cer at 1-4 h treatment was measured, compared to vehicle-treated controls, using the SeaHorse. Data shown are an average of at least two independent experiments performed in duplicates ± s.d. (*$P$ <0.05). **(b)** Effects of $C_{18}$-dihydro-Cer-14-piperidine (Dihydro-C18PC) on MTG/LTR co-localization were determined by confocal microscopy, compared to vehichle-treated controls. **(c)** Possible roles of $C_{18}$-Pyr-Cer (10 $\mu$M) treatment in the alteration of lysosomal flux was examined by determining the co-localization (right panel) of MTG (left panel) and LTR (middle panel) in the absence/presence of bafilomycin (10 nM) compared to vehicle-treated controls (middle, lower and upper panels, respectively). Scale bars represent 10 microns in (b) and (c). **(d)** Effects of stable knockdown of LC3B using shRNAs on LC3B-II formation in the absence/presence of CerS1/C18-ceramide induction (-/+T) was determined by Western blotting, and fold increase in LC3B-II levels were quantified using the ImageJ. Data shown are an average of at least two independent experiments ± s.d. (*$P$ <0.05).

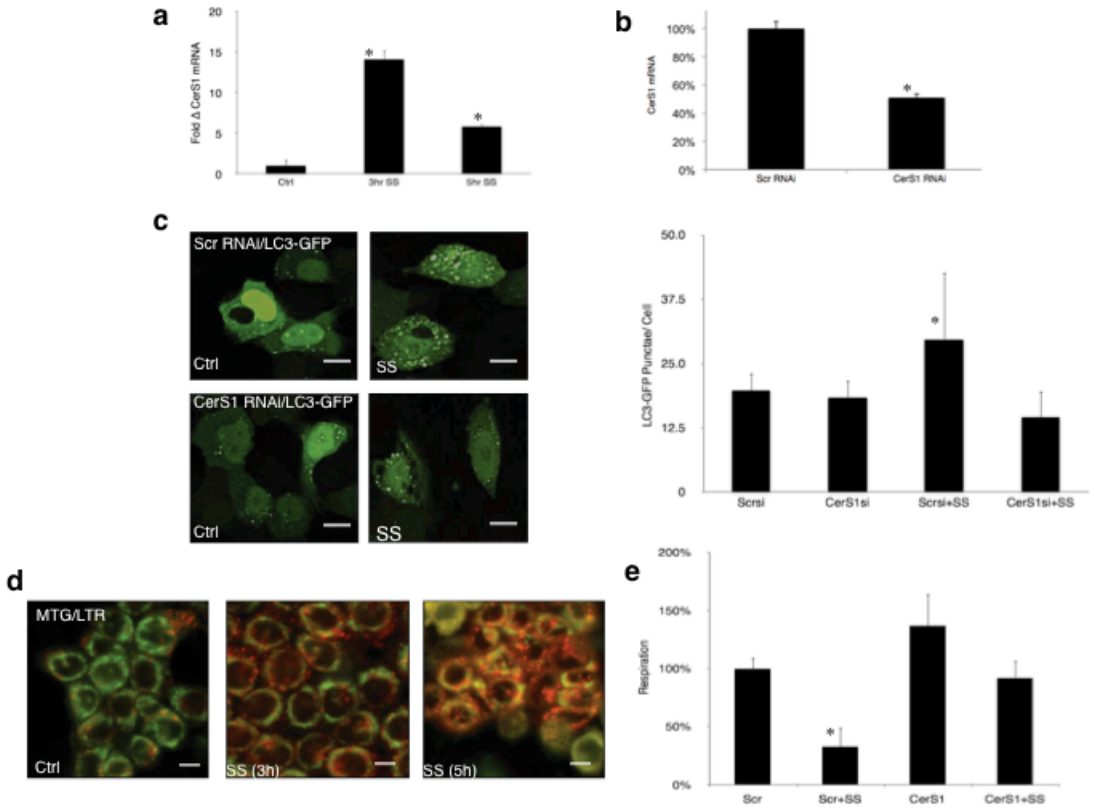


**Supplementary Figure 3.** CerS1/$C_{18}$-ceramide plays key roles in mediating sodium selenite (SS)-induced mitophagy. **(a)** Effects of SS at 3 and 5 h treatment on CerS1 mRNA were measured by Q-PCR, compared to vehicle-treated controls. **(b)** Efficient knockdown of CerS1using siRNAs was measured using Q-PCR in UM-SCC-22A cells compared to Scr-siRNA-transfected controls. Data shown are an average of at least two independent experiments performed in duplicates ± s.d. (*$P$ <0.05). **(c)** Induction of LC3B-GFP lipidation by SS in response to siRNA-mediated knockdown of endogenous CerS1/$C_{18}$-ceramide was visualized by confocal microscopy, compared to controls which were transfected with non-targeting Scr siRNAs. Scale bars represent 10 microns. **(d)** Targeting of mitochondria by autophagolysosomes in response to SS was visualized by co-localization of MTG and LTR using confocal microscopy. Scale bars represent 10 microns. **(e)** Effects of SS treatment on mitochondrial function were examined by measuring OCR using the SeaHorse in the absence/presence of siRNAs against CerS1, compared to Scr siRNA controls. Data shown are an average of at least three independent experiments performed in duplicates ± s.d. (*$P$ <0.05).

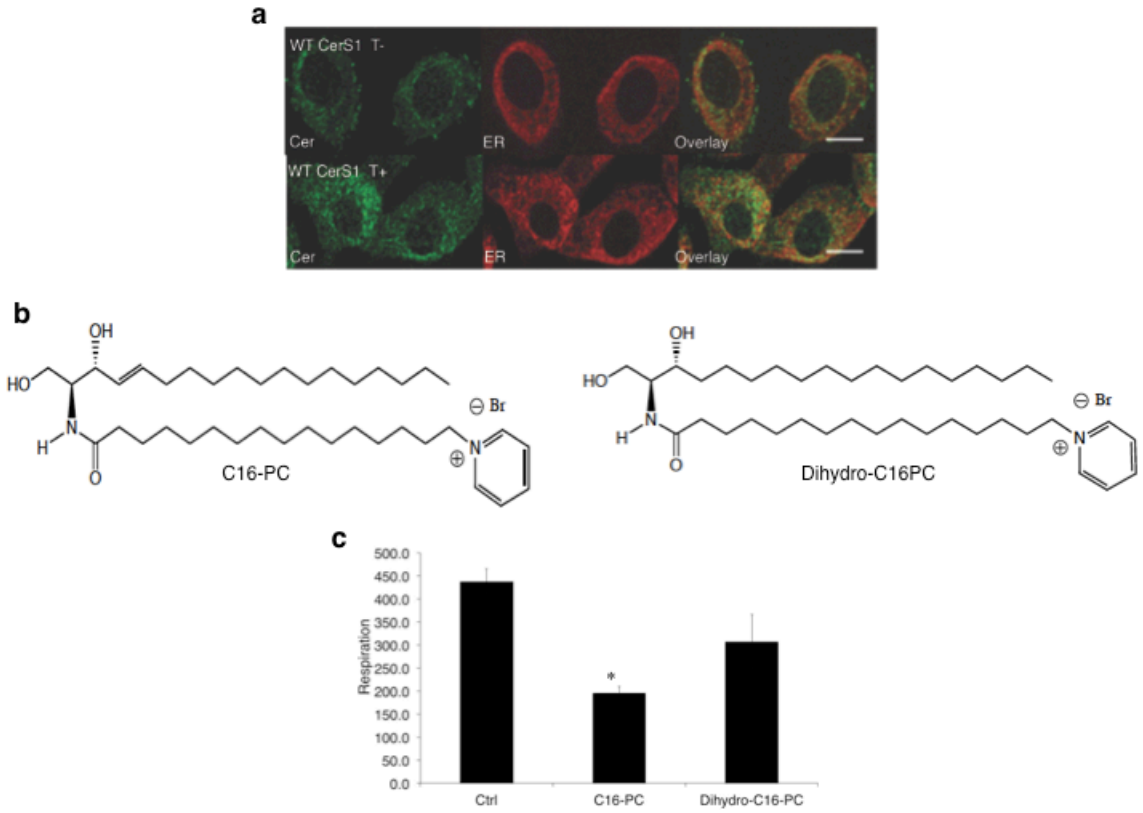


**Supplementary Figure 4.** Subcellular localization of endogenous ceramide, or mitochondrial $C_{16}$-Pyr-Cer versus dihydro-$C_{16}$-Pyr-Cer affects mitochondrial function. **(a)** Effects of wt-CerS1 induction (+tet) on subcellular localization of ceramide in ER were measured using anti-ceramide and anti-calreticulin antibodies, respectively, using confocal microscopy. Scale bars represent 10 microns. **(b-c)** Effects of $C_{16}$-Pyr-Cer (C16-PC) or dihydro-$C_{16}$-Pyr-Cer (Dihydro-C16-PC) (b, left and right panels, respectively) on OCR (c) was measured using the SeaHorse in UM-SCC-22A cells. Data shown are an average of at least three experiments ± s.d. (*$P$ <0.05).

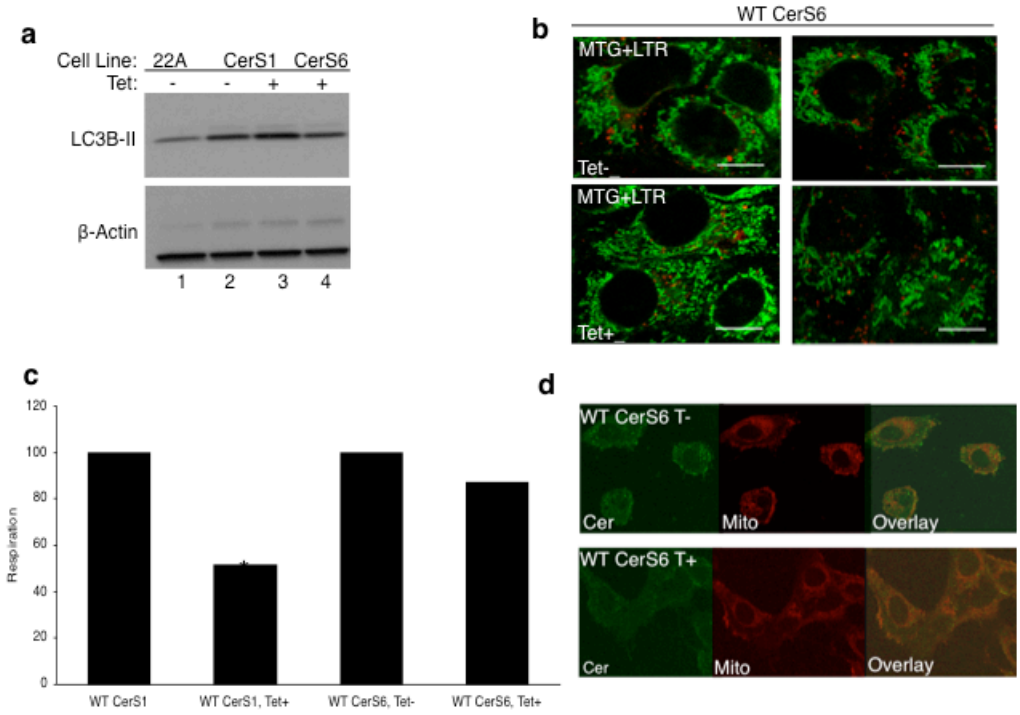


**Supplementary Figure 5.** Cers6 induction, which generates mainly $C_{16}$-ceramide, does not induce mitophagy. **(a)** Lipidation of LC3B in response to CerS1 versus CerS6 induction (+ tet) were examined by Western blotting, compared to controls (lanes 3-4, 1 and 2, respectively). Beta-actin was used as a loading control. **(b)** Effects of CerS6/$C_{16}$-ceramide induction (+ tet) on LC3B-GFP lipidation were determined by confocal microscopy. Non-induced cells were used as controls (- tet). Scale bars represent 10 microns. **(c)** Mitochondrial function in the absence/presence of CerS1/$C_{18}$-ceramide versus CerS6/$C_{16}$-ceramide induction (-/+ tet) were measured using the SeaHorse. Data shown are an average of at least three experiments ± s.d. (*$P$ <0.05). **(d)** Localization of ceramide and MTG using anti-ceramide antibody in response to CerS6 expression was examined by confocal microscopy. Scale bars represent 10 microns.

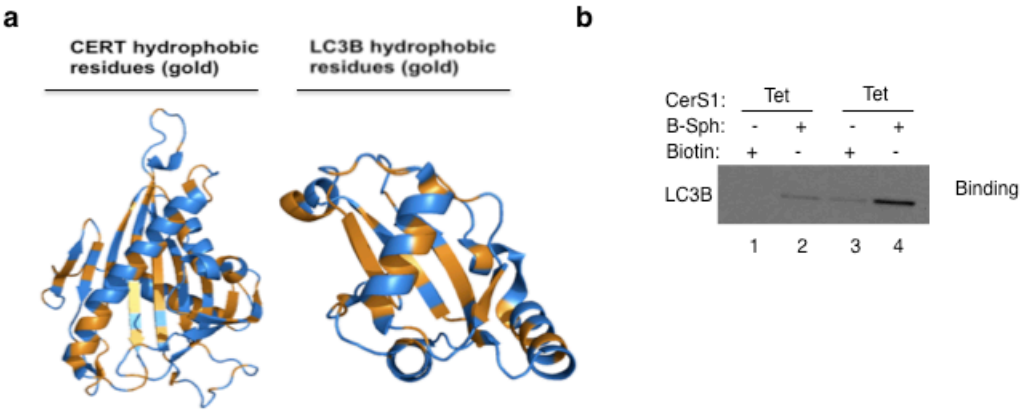


**Supplementary Figure 6.** Structural comparison of hydrophobic lipid-binding domains of CERT versus LC3B. **(a)** Ceramide-binding hydrophobic domain of CERT showed some structural similarities with a central hydrophobic pocket of LC3B (left and right panels, respectively, in gold). **(b)** Binding of biotin-$C_{18}$-ceramide with endogenous LC3B following labeling cells with B-Sph and induction of wt-CerS1 (+ tet) was determined as described in Methods. Non-induced (- tet) cells were used as controls. In these experiments, biotin-$C_{18}$-ceramide-bound proteins were pulled-down using avidin-conjugated beads, and after elution, proteins were resolved by SDS-PAGE before Western blotting.

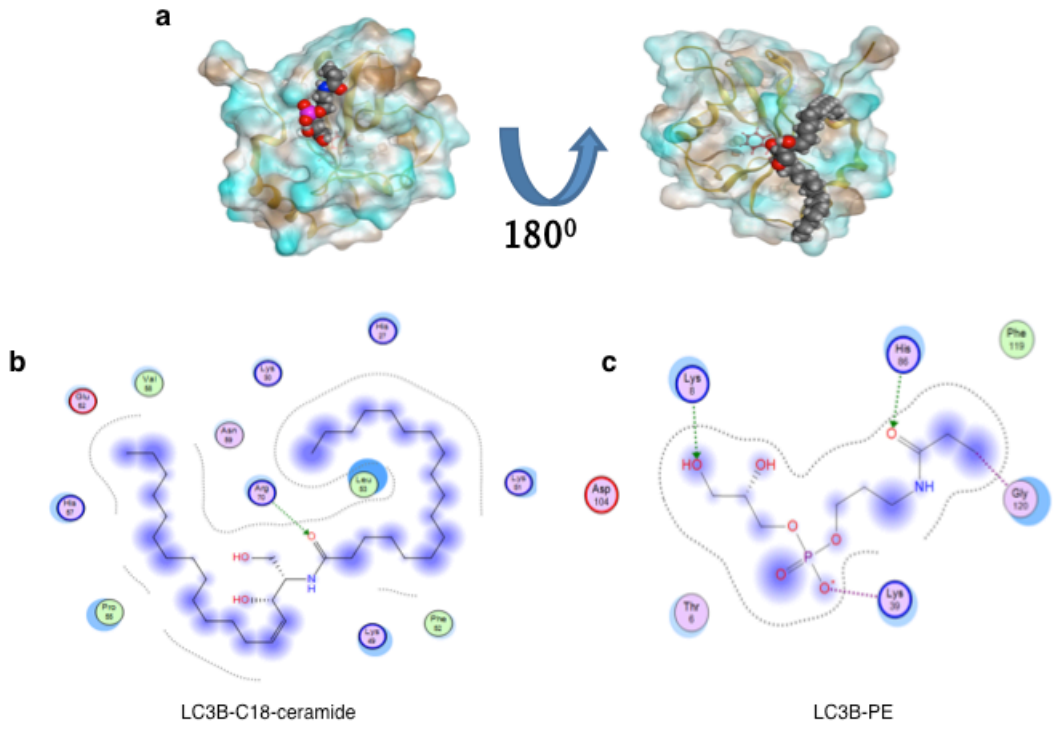


**Supplementary Figure 7**. Analysis of the potential ceramide and PE binding domains of LC3B. **(a)** Predicted ceramide and PE binding domains of LC3B were analyzed by molecular modeling and simulations. PE and ceramide are space-filled while LC3B is depicted with a surface colored according to hydrophobicity (left and right panels, respectively). **(b-c)** Interactions diagram of LC3B and $C_{18}$-ceramide (b) or PE (c) binding are shown.

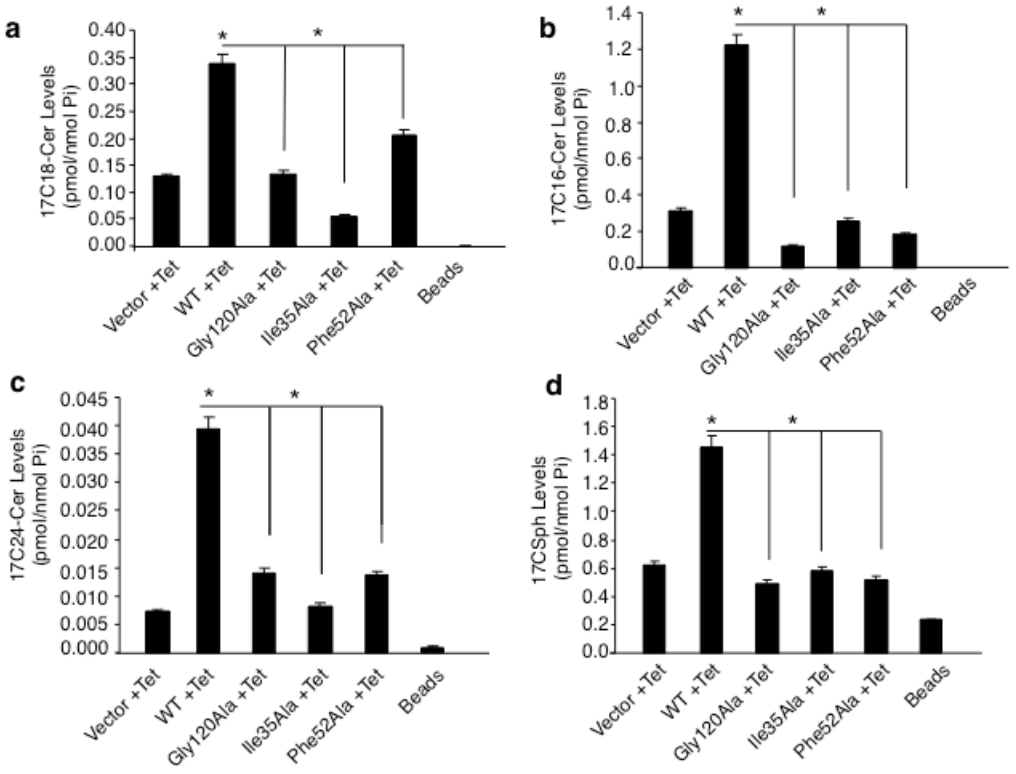


**Supplementary Figure 8**. Measurement of LC3B-II binding to $_{17}$C-Sph-labeled ceramides using LC/MS/MS. **(a-d)** Binding of LC3B-FLAG to endogenously generated $_{17}C_{18}$-, $_{17}C_{16}$, $_{17}C_{24}$-ceramides (a-c, respectively), or $_{17}$C-Sph (d) in the absence/presence of wt-CerS1 induction (-/+ tet) was measured using LC/MS/MS, after LC3B-bound sphingolipids were pulled-down using anti-FLAG antibody-conjugated beads, and after lipid extractions. Ceramide levels were normalized to Pi. Data shown are an average of at least two experiments ± s.d. (*$P$ <0.05).

**a**

| Bound | | | | |
|---|---|---|---|---|
| Avg Norm | 17C16-Cer | 17C18-Cer | 17C24-Cer | 17CSph |
| Vector - Tet | 0.383582 | 0.006644 | 0.011608 | 0.70069 |
| Vector +Tet | 0.312787 | 0.128601 | 0.007305 | 0.62157 |
| WT -Tet | 0.300288 | 0.003829 | 0.010878 | 0.649574 |
| WT +Tet | 1.21958 | 0.33921 | 0.039423 | 1.461262 |
| Gly120Ala +Tet | 0.122282 | 0.132679 | 0.014108 | 0.493469 |
| Ile35Ala +Tet | 0.260893 | 0.054708 | 0.008254 | 0.582978 |
| Phe52Ala +Tet | 0.186704 | 0.203977 | 0.013658 | 0.511037 |

| Flow Through (Unbound) | | | | |
|---|---|---|---|---|
| Avg Normalized | 17C16-Cer | 17C18-Cer | 17C24-Cer | 17CSph |
| Vect -Tet | 14.05079 | 0.32579 | 2.845887 | 0.044248 |
| Vect +Tet | 11.36345 | 4.019834 | 2.987246 | 0.043606 |
| WT -Tet | 15.97527 | 0.401548 | 3.794486 | 0.047093 |
| WT +Tet | 11.16417 | 3.770714 | 3.088251 | 0.048012 |
| Gly120Ala +Tet | 10.99214 | 3.571422 | 3.240957 | 0.038775 |
| Ile35Ala +Tet | 12.76735 | 4.457809 | 3.877944 | 0.036443 |
| Phe52Ala +Tet | 10.93395 | 3.68053 | 3.097457 | 0.048263 |

**b**

| Bound | | | | |
|---|---|---|---|---|
| Avg Norm | 17C14-Cer | 17C20-Cer | 17C22-Cer | 17CS1P |
| Vector - Tet | bd | bd | bd | bd |
| Vector +Tet | bd | bd | bd | bd |

Bd: below detectable

**Supplementary Figure 9.** Analyses of LC3B/ceramide binding using LC/MS/MS. **(a-b)** Binding of LC3B-FLAG (wt, Gly120Ala, Ile35Ala and Phe52Ala) to $_{17}C_{18}$-, $_{17}C_{16}$, $_{17}C_{24}$-ceramides, and $_{17}$C-Sph (a), or $_{17}C_{14}$-, $_{17}C_{20}$, $_{17}C_{22}$-ceramides, and $_{17}$C-S1P (b) in the absence/presence of wt-CerS1 induction (-/+ tet) was measured using LC/MS/MS and normalized to Pi. Data shown are an average of at least two experiments ± s.d.

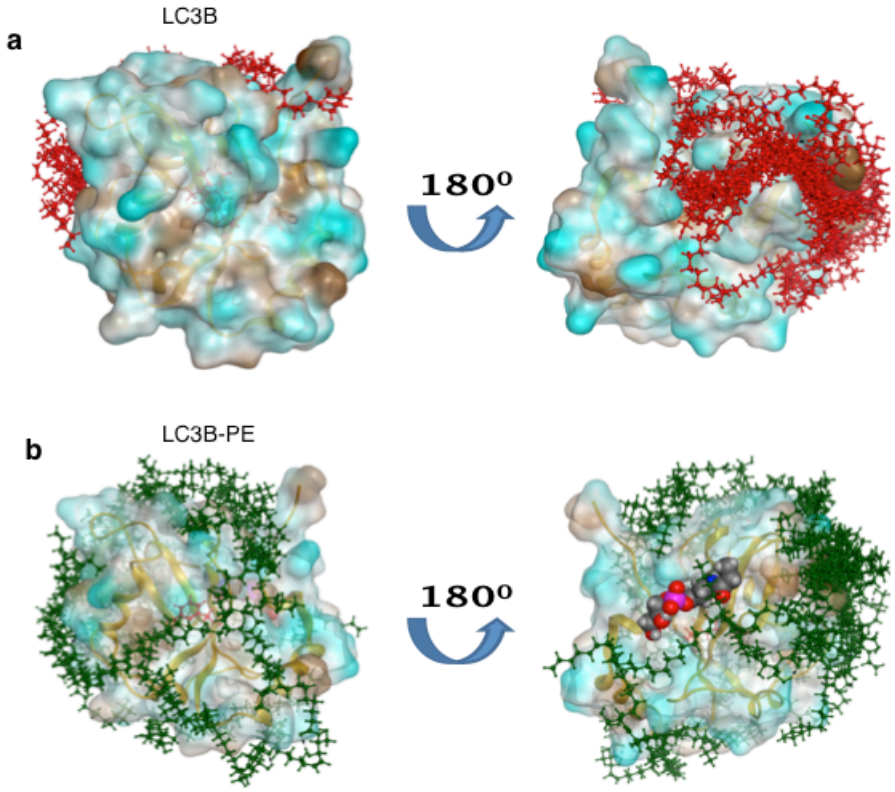


**Supplementary Figure 10.** Docking simulation of ceramide binding to unmodified and PE modified LC3. **(a-b)** The top 30 poses of $C_{18}$-ceramide (red or green) presented according to binding to the unmodified LC3B (a) or PE modified LC3B (b), respectively. The peptide backbone is imaged as a yellow ribbon in all images and Phe52 is visible as the red amino acid in a and b.

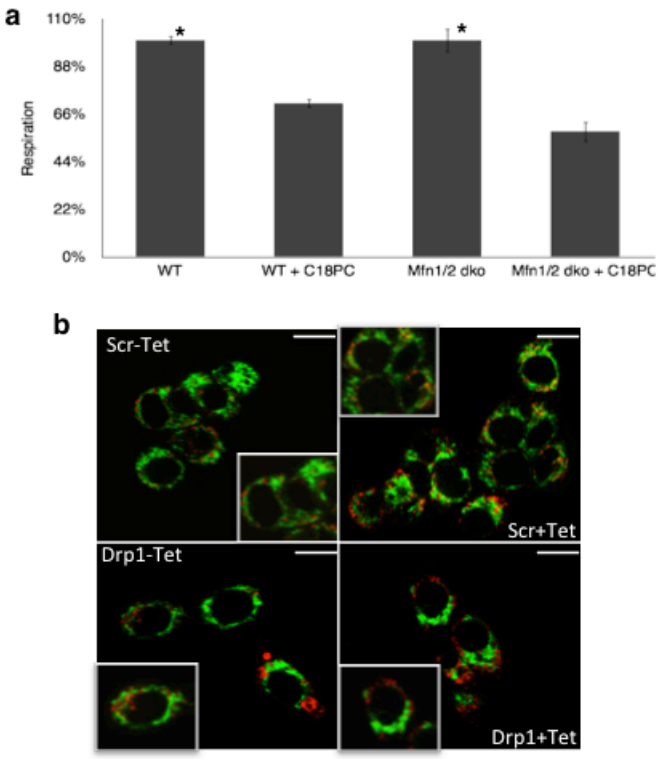


**Supplementary Figure 11**. Effects of mitochondrial fusion versus fission on ceramide-induced mitophagy. **(a)** Effects of genetic loss of mitofusion 1 and 2, which are known regulators of mitochondrial fusion process, on OCR in the absence/presence of $C_{18}$-Pyr-Cer were measured using the SeaHorse, in MEFs isolated from mitofusion1/2-/- dko and wt mice. Data shown are an average of at least three experiments ± s.d. (*$P$ <0.05). **(b)** Effects of siRNA-mediated knockdown of Drp1, a known regulator of mitochondrial fission, on mitophagy were determined by the analyses of MTG and LTR co-localization in the absence/presence of CerS1/$C_{18}$-ceramide induction (-/+Tet), compared to Scr-siRNA-transfected cells under confocal microscopy. Scale bars represent 10 microns.

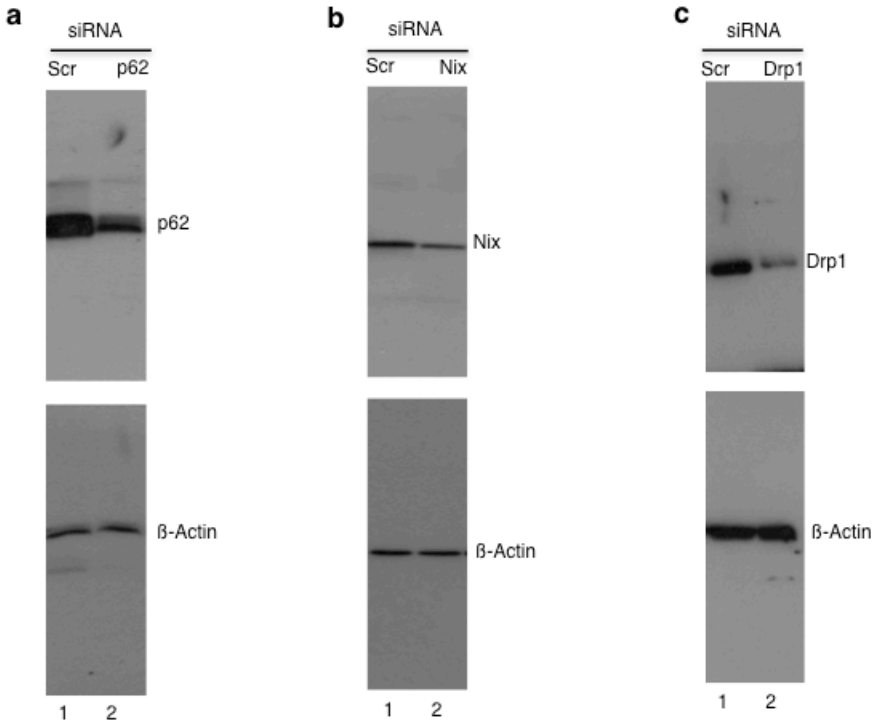


**Supplementary Figure 12**. SiRNA-mediated knockdown of p62, NIX and Drp1 expression. **(a-c)** Efficiency of siRNA-mediated knockdown of p62 (a), NIX (b), and Drp1 (c) was measured using Q-PCR compared to Scr-siRNA-transfected controls (upper panels, lanes 2 and 1, respectively). Beta-actin levels were measured as loading controls.

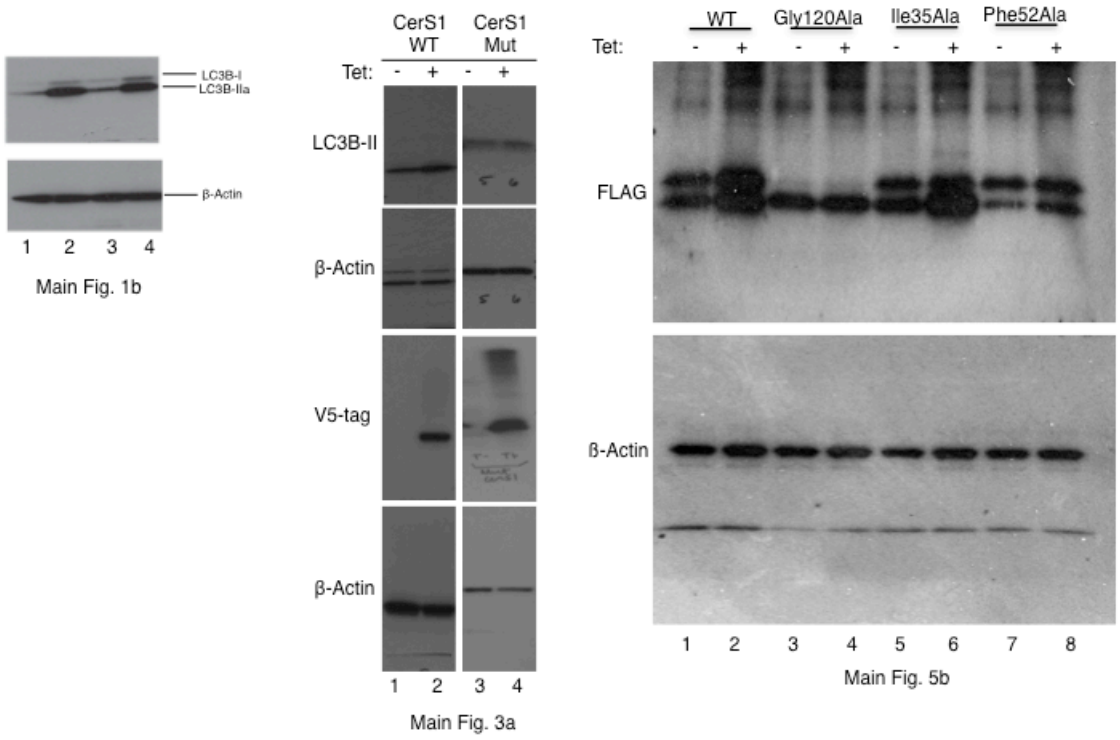


**Supplementary Figure 13.** Full Western blots. Full blots presented in Figures 1b, 3a, 5b are shown.

## SUPLEMENTARY METHODS

**Cells and culture conditions.** UM-SCC 22A hypopharengeal cancer cells stably expressing both wild-type (wt) and the mutant CerS1 or CerS6 under the regulation of a tet-inducible promoter were developed using a lentiviral expression system, and maintained in 1x DMEM, 10% tet-voided fetal bovine serum and 1% penicillin/streptomycin. UM-SCC-22A cells expressing wt-CerS1 were stably transduced with pGIPz LC3B shRNA and non-targeting pGIPz shRNA (Open Biosystems). ATG5-/-, Bax/Bak (dko) and caspase 3/7-/- (dko) MEFs were obtained from Drs. N. Mizushima (Tokyo Medical and Dental University), D. Green (St. Jude Children's Research Hospital), and R.A. Flavell (Yale), respectively.

**Reagents, siRNAs and Transfections.** SS was purchased from Sigma-Aldrich. Cationic ceramides were synthesized at the synthetic Lipidomics Core at MUSC, as described previously[20]. SiRNAs against Cers1, Atg3, Atg7, p62, Nix, and Drp1 were purchased from Dharmacon, and they were used for transfections with Oligofectamine for 48 hr. Non-targeting scrambled siRNAs (Scr) (Dharmacon) were used as controls. Efficiency of siRNAs was evaluated by quantitative real time PCR (Q-PCR) and/or Western blotting. β-actin or rRNA were used as internal controls. Target sequence of LC3B siRNA, targeting 5' UTR was as follows: 5'-GAUACAAGGGAAGUGGCUAUU-3'. Sequences of primers used for generation of wt and mutant LC3B-FLAG expression vectors were as follows: Forward: 5'-GGAATTCCATGGATTACAAGGATGACGACGATAAGCC-GTCGGAGAAGACCTC-3'; Reverse: 5'-CCTCGAGGTTACACTGACAATTTC-3', cloned into pcDNA3.1 between EcoRI and XhoI restriction sites. The following primers

were used to generate I35A, F52A and Gly120A mutants of LC3B: I35A-LC3B, forward: 5'-CAGCATCCAACCAAAATCCCGGTGATAGCAGAACGATACAAGG-3', reverse: 5'-CCTTGTATCGTTCTGCTATCACCGGGATTTTGGTTGGATGCTG-3'. F52A-LC3B, forward: 5'-CCTGTTCTGGATAAAACAAAGGCCCTTGTACCTGACCAT-GTCAA-3', and reverse: 5'-TTGACATGGTCAGGTACAAGGGCCTTTGTTTTATC-CAGAACAGG-3'. G120A-LC3B, forward: 5'-TCCCAGGAGACGTTCGCGAT-GAAATTGTCAGTG-3', reverse: 5'-CACTGACAATTTCATCGCGAACGTCT-CCTGGGA -3'.Transfections were performed using Effectine, and expression of proteins were measured by Western blotting.

**Molecular Modeling and Docking Simulations.** Modeling, simulations and visualizations were performed using MOE Version 2010.10 (CCG). Simulations were performed on a Dell E8500 with an Intel Core 2 Duo @ 3. 16GHz using a Windows XP OS. The structural pbd file used as input for LC3b was pdb 1V49 (PubMed: 15857831). Before analysis and simulations the LC3B protein was protonated at pH 7.5/Salt 0.2M using the Generalized Born/Volume Integral implicit solvent model. The structure was then energy minimized using MMFF94x forcefield without tethering constraints to create the unmodified docking target. To create the PE modified LC3B, phosphatidyl-ethanolamine (PE) was covalently bonded to the exposed Gly120. The PE modification was manually rotated to close proximity of the main chain protein and the system energy minimized again to provide the PE modified LC3B model. Computational docking of $C_{18}$-ceramide to LC3B models consisted of two phased docking simulations. For both models initial placement calculation for 300 poses using triangle matching with London

dG scoring was performed and the top 100 poses were then refined using forcefield based refinement and affinity dG scoring.

**Measurement of ATP.** ATP levels were quantified using the Cell Titer Glo Luminescent Cell Viability Assay (Promega), as described by the manufacturer.

**Measurement of xenograft-driven tumor growth *in vivo*.** Roles of LC3B knockdown in the absence/presence of tet-induced CerS1 expression in the regulation of tumor progression and/or growth *in vivo* were determined by implantation of 6 x$10^6$ UMSCC-22A/wt-CerS1/sh-Control or wt-CerS1/sh-LC3B cells into the flanks of SCID mice (n=6 tumors/group) as described[21,34]. After tumors reached to 50-100 $mm^3$ volume, animals were exposed to 1 mg/ml doxycycline for 28 days. Tumor formation was evaluated at every 3 days for 28 days using calipers as described previously. Protocols used in animal studies were approved by the Institutional Animal Care and Use Committee (IACUC) at the Medical University of South Carolina.

**Statistical analysis.** Student's t-test was used to analyze the data, and $P < 0.05$ (*) was regarded as significant.